Galaxy Environments over Cosmic Time: The Non-evolving Radial Galaxy Distributions around Massive Galaxies since z = 1.6

Tal, T.; Dokkum, P.G. van; Franx, M.; Leja, J.; Wake, D.; Whitaker, K.

The Astrophysical Journal, 769:31 (8pp), 2013 May 20 doi:10.1088/0004-637X/769/1/31

GALAXY ENVIRONMENTS OVER COSMIC TIME: THE NON-EVOLVING RADIAL GALAXY DISTRIBUTIONS AROUND MASSIVE GALAXIES SINCE $z = 1.6$

Tomer Tal[1,6], Pieter G. van Dokkum[2], Marijn Franx[3], Joel Leja[2], David A. Wake[4], and Katherine E. Whitaker[5]
[1] UCO/Lick Observatory, University of California, Santa Cruz, CA 95064, USA; tal@ucolick.org
[2] Yale University Astronomy Department, P.O. Box 208101, New Haven, CT 06520-8101 USA
[3] Leiden Observatory, Leiden University, NL-2300 RA Leiden, The Netherlands
[4] Department of Astronomy, University of Wisconsin-Madison, Madison, WI 53706, USA
[5] Astrophysics Science Division, Goddard Space Flight Center, Greenbelt, MD 20771, USA
Received 2013 February 6; accepted 2013 April 3; published 2013 May 2

ABSTRACT

We present a statistical study of the environments of massive galaxies in four redshift bins between $z = 0.04$ and $z = 1.6$, using data from the Sloan Digital Sky Survey and the NEWFIRM Medium Band Survey. We measure the projected radial distribution of galaxies in cylinders around a constant number density selected sample of massive galaxies and utilize a statistical subtraction of contaminating sources. Our analysis shows that massive primary galaxies typically live in group halos and are surrounded by 2–3 satellites with masses more than one-tenth of the primary galaxy mass. The cumulative stellar mass in these satellites roughly equals the mass of the primary galaxy itself. We further find that the radial number density profile of galaxies around massive primaries has not evolved significantly in either slope or overall normalization in the past 9.5 Gyr. A simplistic interpretation of this result can be taken as evidence for a lack of mergers in the studied groups and as support for a static evolution model of halos containing massive primaries. Alternatively, there exists a tight balance between mergers and accretion of new satellites such that the overall distribution of galaxies in and around the halo is preserved. The latter interpretation is supported by a comparison to a semi-analytic model, which shows a similar constant average satellite distribution over the same redshift range.

Key words: galaxies: elliptical and lenticular, cD – galaxies: groups: general

Online-only material: color figures

1. INTRODUCTION

The properties of galaxies in the nearby universe are strongly affected by the environment in which they reside. Morphology, mass, star formation rates, and stellar colors of individual galaxies have all been shown to be correlated with the local galaxy density (e.g., Oemler 1974; Dressler 1980; Kauffmann et al. 2004; Hogg et al. 2004; Blanton et al. 2005; Thomas et al. 2005; Clemens et al. 2006; Andreon et al. 2006; van den Bosch et al. 2008; Skibba & Sheth 2009; Peng et al. 2010; Zehavi et al. 2011; Quadri et al. 2012). Therefore, significant effort has been devoted to studies of galaxy environments at low and high redshift, utilizing a number of approaches (e.g., Zehavi et al. 2002; Madore et al. 2004; Mandelbaum et al. 2006; Holden et al. 2007 Gavazzi et al. 2007; Bolton et al. 2008; Wake et al. 2008, 2011; Patel et al. 2009, 2011; Cacciato et al. 2013; Knobel et al. 2012; Diener et al. 2013). Nevertheless, the density and distribution of galaxies in groups, where nearly all massive galaxies are expected to reside, are still poorly known at $z > 1$. At this redshift, it is difficult to uniquely match galaxies to halos except in the most overdense regions.

Recently, a number of studies analyzed the small-scale clustering of satellite galaxies around massive primaries (the most massive galaxies in their halos) using statistical tools. By utilizing large data sets and statistical background subtraction, authors were able to extract satellite galaxy distributions from observational and numerical catalogs. For example, Masjedi et al. (2006, 2008), Watson et al. (2012), and Tal et al. (2012a) examined the radial profile of dark matter halos around primary galaxies and found that they become steeper on very small scales. Quilis & Trujillo (2012) and Budzynski et al. (2012) compared the observed distribution of satellite galaxies to results from numerical simulations and semi-analytic models and showed that numerical predictions typically overestimate the abundance of satellites at both low and high redshift. Guo et al. (2013) compared the colors of observed and modeled satellite galaxies and found that satellites in semi-analytic models have redder colors than their observed counterparts.

Interestingly, statistical studies of satellite galaxies around massive primaries found no significant correlation between the radial distribution of satellites and the properties of their host galaxy. Nierenberg et al. (2012) and Jiang et al. (2012) found that the shape and slope of the radial profile of satellite galaxies do not vary with host properties and satellite luminosity. Wang & White (2012) showed that the stellar mass function of such satellite galaxies is similar in shape to that of field galaxies. Mármol-Queraltó et al. (2012, 2013) used statistical background subtraction to show that the fraction of massive primaries that have massive satellites around them remains essentially constant out to $z = 2$.

Here we follow a statistical approach to derive the radial distribution of satellite galaxies around a constant cumulative number density selected sample of massive primaries. We extract average projected galaxy profiles out to $z = 1.6$ for the first time and trace their evolution over the past 9.5 billion years in a self-consistent way.

Throughout the paper we adopt the following cosmological parameters: $\Omega_m = 0.3$, $\Omega_\Lambda = 0.7$ and $H_0 = 70$ km s^{-1} Mpc^{-1}.

2. SAMPLE SELECTION

We utilized data from two public surveys for this study, from the Sloan Digital Sky Survey (SDSS; York et al. 2000) and from the NEWFIRM Medium Band Survey (NMBS; van

[6] NSF Astronomy and Astrophysics Postdoctoral Fellow.

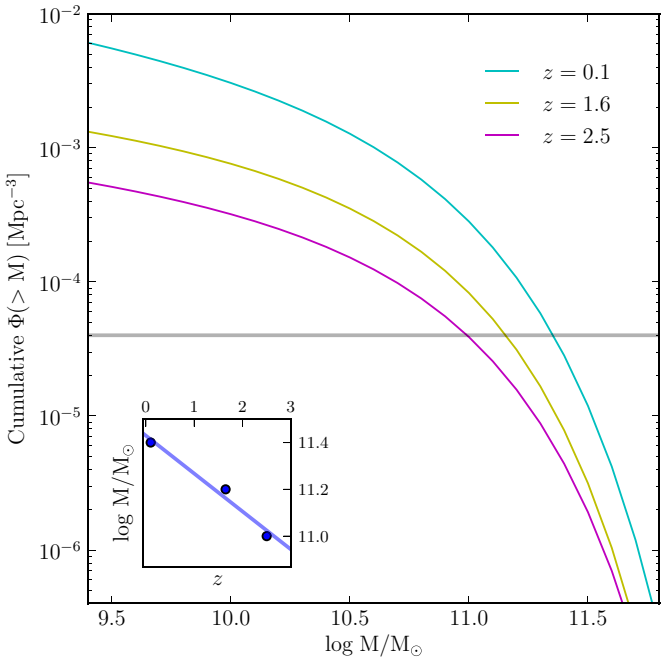

Figure 1. Sample matching of the four redshift bins. The teal, yellow, and magenta lines represent the cumulative mass functions of Marchesini et al. (2009). We calculated galaxy masses at a constant cumulative number density of 4×10^{-5} Mpc^{-3} (gray line) and derived a mass-redshift relation (inset figure). We then selected galaxies in log M bins according to the derived relation.

(A color version of this figure is available in the online journal.)

Dokkum et al. 2009; Whitaker et al. 2011). Galaxies in three redshift bins in the range $0.4 < z < 1.6$ were selected from NMBS, a deep imaging program with the NOAO Extremely Wide-Field Infrared Imager. The total imaging area of NMBS spans roughly 0.39 deg^2 over two fields and the catalogs include tens of thousands of galaxies for which excellent photometric redshifts were calculated ($\sigma_z/(1+z) \sim 0.02$; Brammer et al. 2009). Low redshift galaxies were selected at $0.04 < z < 0.07$ from the MPA-JHU emission line analysis catalogs[7] which are based on the seventh data release of SDSS (Abazajian et al. 2009).

2.1. Cumulative Number Density Matching

Studies of galaxy evolution often match their samples such that galaxies at all redshifts have similar observed properties (e.g., constant stellar mass, luminosity). However, the masses and luminosities of galaxies are expected to evolve and change with time. Alternatively, samples can be matched based on their number density, regardless of galaxy properties. Since cumulative number density is not expected to change dramatically even with a non-negligible number of mergers (e.g., Gao et al. 2004; van Dokkum et al. 2010; Papovich et al. 2011; Patel et al. 2013; Leja et al. 2013), this approach essentially follows the evolution of observed properties of a given galaxy population. We utilized the latter technique to match massive galaxy populations in the two data sets in four redshift bins.

We started by adopting the model fits to the mass functions from Marchesini et al. (2009) to calculate the cumulative number density of three redshift samples as a function of stellar mass (Figure 1). We then fit a line to the mass-redshift relation of galaxies at a constant number density of 4×10^{-5} Mpc^{-3} and found the following mass evolution with redshift:

$$\log(M_\star/M_\odot) = -0.16z + 11.43 \quad (1)$$

The best-fit relation implies doubling of stellar mass in the last 9.5 Gyr for these galaxies and it is consistent with other mass evolution studies (e.g., van Dokkum et al. 2010). We selected primary galaxy candidates in log $M_\star$ bins of width 0.3 dex with an evolving median mass according to Equation (1). Galaxies were considered to be "primary" if no other, more massive, galaxies were found within a projected radius of 500 kpc. Otherwise, they were counted as "satellites" of their more massive neighbor. The redshift limits for this study were determined such that the samples from both surveys were complete down to one-tenth of the stellar mass of all selected primaries. Redshift bin sizes were chosen to have roughly equal volumes in the three NMBS bins and to maximize the number of galaxies from SDSS, whilst remaining complete in stellar mass.

A summary of the selected samples is given in Table 1.

Table 1
Galaxy Properties in the Four Selected Redshift Bins

Data Set	z	V (Mpc^3)	log ($M_{\rm med}/M_\odot$)	$N_{\rm P}$
SDSS	$0.04 < z < 0.07$	1.6×10^7	11.42	360
NMBS	$0.4 < z < 0.9$	9.8×10^5	11.33	44
	$0.9 < z < 1.3$	1.4×10^6	11.25	89
	$1.3 < z < 1.6$	1.2×10^6	11.20	97

3. RADIAL NUMBER DENSITY PROFILES

Various techniques are commonly used to quantify galaxy environments at low and high redshift. Here we perform an analysis of the distribution of objects around the selected galaxies and subtract the contribution of background and foreground sources in a statistical manner. One of the advantages of this method is that it does not rely on a priori assumptions regarding the total mass or size of the host dark matter halo.

3.1. Profile Derivation

We started by selecting all galaxies in the NMBS catalog that were within $\Delta z \leqslant 0.2$ of the measured redshift of the massive primaries and within $\Delta z \leqslant 0.005$ in the SDSS MPA-JHU catalog. From this selection we excluded all galaxies whose mass was less than one-tenth of their corresponding primary mass. We then derived the radial number density galaxy profiles by binning the selected galaxies in log-radial bins (blue lines in Figure 2).

The resulting radial number density profiles include galaxies that are physically associated with each primary as well as sources in the background and foreground. In order to account for this contamination we repeated the derivation in randomly selected positions within the entire survey area and calculated the average radial profile of contaminating sources (red lines in Figure 2). Finally, we subtracted the average random profile from the average primary profile at each redshift to derive the cylindrical distribution of physically associated galaxies around massive primaries.

The radial distribution of galaxies around massive primaries out to $z = 1.6$ is shown in Figure 3, where the density of physically associated galaxies is plotted as a function of projected physical distance from the primary. The blue line represents the measurement at $0.04 < z < 0.07$ from SDSS

[7] http://www.mpa-garching.mpg.de/SDSS/DR7/

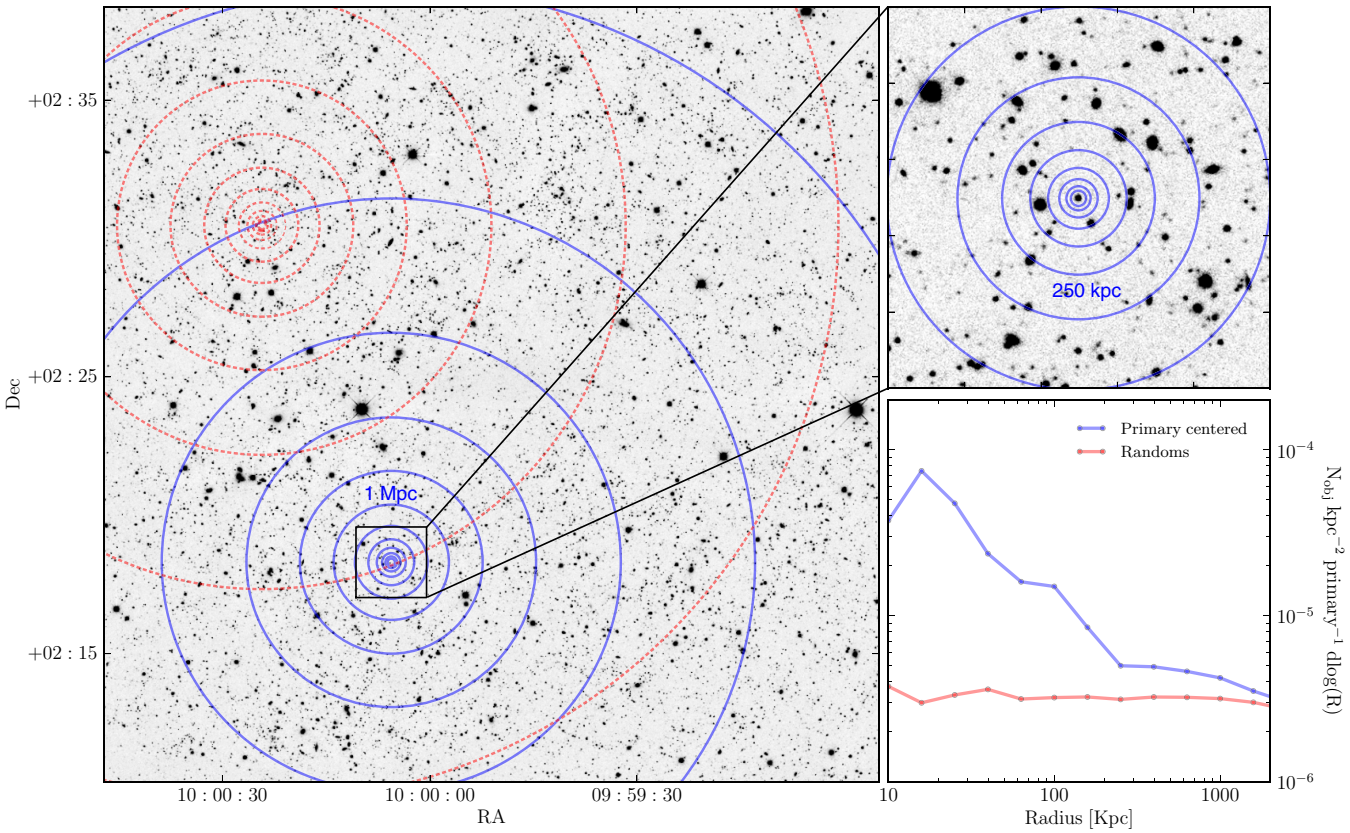

Figure 2. Demonstration of the radial number density profile extraction technique. We divided catalog sources into log(r) bins around the selected primaries (blue lines) and around randomly selected positions in the field (red lines). The bottom-right panel shows an example of the stacked radial profiles of all galaxies at $1.3 < z < 1.6$. The projected radial profiles of galaxies around the selected primaries were revealed by subtracting the average random profile from the galaxy-centered profile.

(A color version of this figure is available in the online journal.)

while the yellow, green, and red lines show the three higher redshift bins from NMBS. We note that the lowest redshift profile (blue line) is not plotted at $r < 55''$ (roughly 74 kpc at $z = 0.07$), where the spectroscopic catalog of SDSS is incomplete due to fiber collisions.

3.2. Error Estimates

The range of measured number density values in the random profiles reflects the statistical variation of the overall galaxy distribution throughout the survey fields. In addition to averaging all random profiles in each redshift bin, we also calculated the standard deviation of the distribution of individual profiles as a function of radius. This measurement depicts the statistical uncertainty in our calculations.

In addition to statistical errors, a number of systematic uncertainties may potentially affect our results in a non-trivial way. For example, uncertainties in mass and redshift measurements may move galaxies in and out of a given redshift sample and therefore change the profile normalization and slope. In the innermost radii the profiles may be underestimated due to source blending close to the bright primaries. While redshift errors in NMBS are well quantified and are expected to have a minor effect on the number density profiles, uncertainties in stellar mass measurements are complex and depend on a large number of fitting parameters (e.g., Marchesini et al. 2009; Muzzin et al. 2009; Conroy et al. 2009).

We quantified the effect of redshift errors by scattering all measured redshifts in the NMBS catalog by a normal distribution with width $\sigma_z/(1+z) = 0.02$. This value represents the scatter in the relation between photometric and spectroscopic redshift measurements in NMBS as was found by Brammer et al. (2009). We extracted number density profiles using the scattered catalog, following the procedure described in Section 3.1. The overall shape and normalization of the resulting profiles are consistent with the non-scattered profiles and the resulting errors are within ±20% of the above derived statistical errors at all radii.

We also estimated the effect of errors in stellar mass derivations by introducing an additional normally distributed scatter with $\sigma_M = 0.3$ dex to the mass of all galaxies in the NMBS catalogs. This value, which is identical to the width of our selection mass bin, was chosen to represent an upper limit on typical errors of stellar mass estimates. The additional scatter tests how our results are affected by moving primary galaxies above and below the mass selection thresholds. We repeated the number density extraction technique once again and derived mass related error estimates based on the range of resulting values. The effect of mass errors is more significant than the effect of both statistical and redshift measurement errors. In addition, the resulting error estimates are asymmetric around the number density profiles since galaxies close to the lower mass threshold of the survey can only be scattered out of our selection.

The error bars in Figure 3 represent statistical uncertainties as well as redshift and mass estimate errors in this study.

Measured values and error estimates that are presented in Figure 3 are given in Table 2.

3.3. Profile Dependence on Primary Mass

In order to test whether our results are sensitive to the mass of the primaries we divided the $0.9 < z < 1.3$ sample into

Table 2
Projected Radial Profile Measurements

log(R)[a]	$0.04 < z < 0.07$		$0.4 < z < 0.9$		$0.9 < z < 1.3$		$1.3 < z < 1.6$	
	log(ϕ)[b]	log($\Delta\phi$)[c]	log(ϕ)[b]	log($\Delta\phi$)[c]	log(ϕ)[b]	log($\Delta\phi$)[c]	log(ϕ)[b]	log($\Delta\phi$)[c]
1.2					−4.14	−5.16	−4.10	−5.02
1.4			−4.35	−5.23	−4.35	−5.36	−4.31	−5.28
1.6			−4.26	−5.47	−4.70	−5.60	−4.79	−5.41
1.8			−5.01	−5.61	−4.89	−5.71	−4.78	−5.63
2.0	−5.20	−5.69	−4.78	−5.76	−4.93	−5.97	−5.07	−5.80
2.2	−5.34	−6.30	−5.03	−5.98	−5.28	−6.11	−5.38	−6.00
2.4	−5.60	−6.32	−5.29	−6.07	−5.73	−6.31	−5.45	−6.23
2.6	−5.82	−6.52	−5.44	−6.24	−5.77	−6.42	−5.69	−6.34
2.8	−6.06	−6.63	−5.71	−6.37	−5.86	−6.56	−5.65	−6.44
3.0	−6.26	−7.09	−5.94	−6.45	−5.98	−6.71	−5.78	−6.55
3.2	−6.52	−6.99	−6.02	−6.55	−6.29	−6.88	−5.95	−6.61
3.4	−6.70	−7.17	−6.21	−6.71	−6.53	−6.88	−6.11	−6.73
3.6	−7.09	−7.37	−6.40	−6.81	−7.15	−7.01	−6.38	−6.79

Notes.
[a] Central value of the logarithmic radius bin.
[b] Logarithm of the average projected galaxy density in units of $N_{\rm gal}$ kpc^{-2} primary^{-1} $d\log(R)$.
[c] Logarithm of the estimated error of the average projected galaxy density.

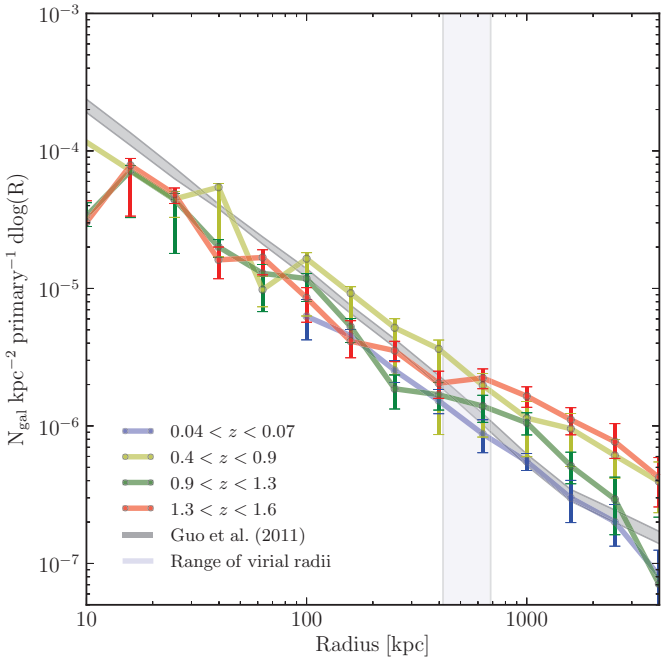

Figure 3. Projected radial profile of galaxies around the selected primaries in four redshift bins (colored lines). The profiles show a remarkable lack of evolution in the radial galaxy distribution since $z = 1.6$. The shaded gray profile represents a similar derivation using the semi-analytic model of Guo et al. (2011), over the same redshift range. The vertical light gray area shows the range of virial radius values of the dark matter halos containing the modeled galaxies. The observed profiles are consistent with the modeled ones over most of the radial range.

(A color version of this figure is available in the online journal.)

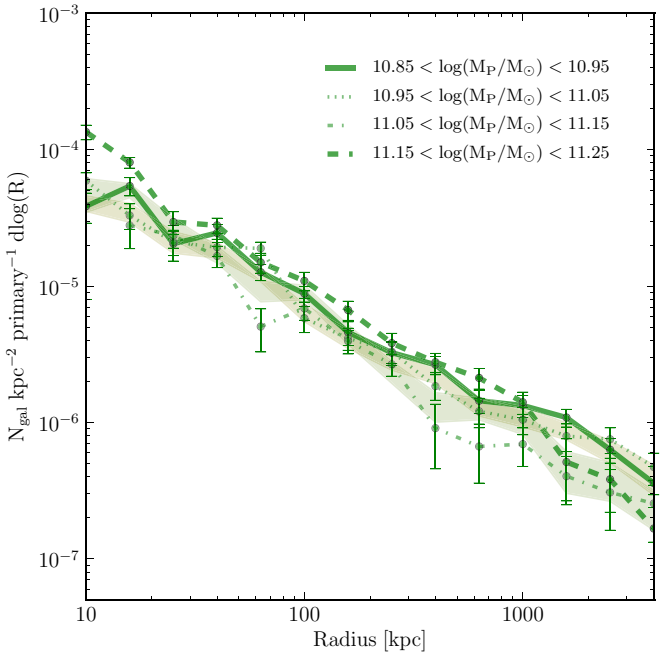

Figure 4. Projected radial number density profiles in the redshift range $0.9 < z < 1.3$ in four mass bins (green lines and error bars). The thick lines highlight the radial distribution of galaxies around the most massive and least massive primaries. The shaded regions represent the resulting number density profiles and errors from utilizing two, rather than four, mass bins. We found no evidence for a strong dependence on the primary galaxy mass within the probed mass range.

(A color version of this figure is available in the online journal.)

four bins according to the total stellar mass of the primary galaxies. We selected primaries with masses in the range $10.85 < \log(M_P/M_\odot) < 11.25$ and calculated the radial number density profile of each mass bin following the method described in Section 3. We estimated the statistical uncertainties for each mass bin using the variation in individual profile measurements. Figure 4 shows that the radial number density profiles of all four mass bins are consistent with one another and no strong mass dependence is apparent in this sample. However, we note that the relatively small mass range of selected primaries may be insufficient to detect even a moderate mass dependence.

3.4. Environment of Massive Primaries

In order to calculate the mass density in the vicinity of our sample primaries we converted the number density profiles from Figure 3 into a cumulative number of satellites as a function of radius. Figure 5 shows the integrated curves of the NMBS profiles as a function of integration radius. The top x-axis of the figure shows the orbital timescale of a test particle in a

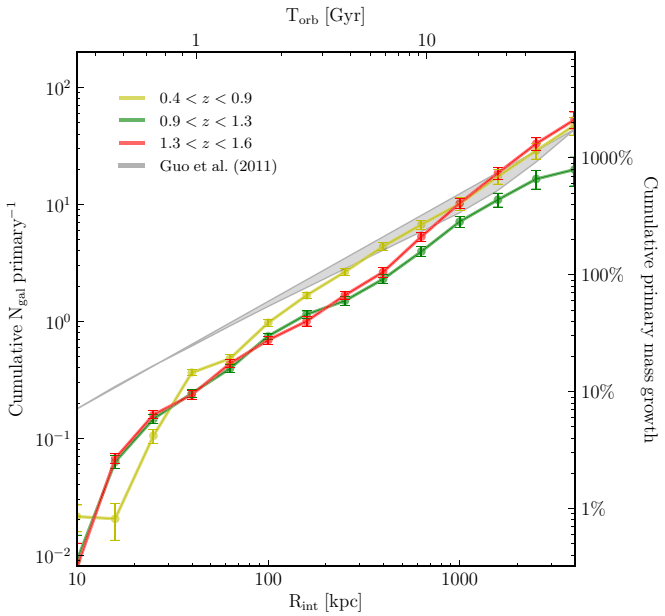

Figure 5. Cumulative number of galaxies as a function of integration radius from NMBS (solid yellow, green, and red lines) and from G11 (gray shaded region). The upper *x*-axis shows an estimate of the orbital time scale under an assumed NFW halo with total mass $2 \times 10^{13}\ M_{\odot}$. The right-hand *y*-axis displays the radially integrated galaxy mass, assuming that all galaxies have the median mass of 40% of their respective primary mass. Primary galaxies can double in mass by merging with 2.5 galaxies that are at $r \lesssim 300$ kpc.

(A color version of this figure is available in the online journal.)

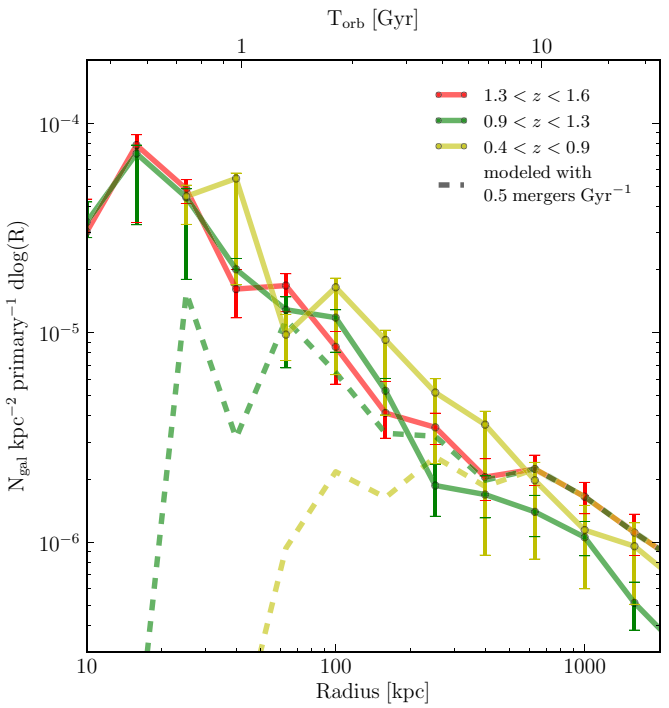

Figure 6. Estimates of the effect of in-halo mergers on the radial number density profile evolution. We modeled mergers by excluding galaxies from the derived profiles of each primary galaxy in the range $10 < r/\mathrm{kpc} < 400$. The dashed lines represent the expected evolution of the $1.3 < z < 1.6$ profile into subsequent redshift bins at a merger rate of 0.5 Gyr^{-1} with no external halo accretion.

(A color version of this figure is available in the online journal.)

spherical halo with total mass $2 \times 10^{13} M_{\odot}$ which is distributed as a Navarro et al. (1997, NFW) profile. The *y*-axis on the right-hand side of Figure 5 represents an estimate of the total enclosed mass as a function of radius, assuming that the mass of each plotted galaxy equals 40% of its primary mass. This value represents the median mass of all selected galaxies as calculated from the global mass function at $z = 1.6$.

Average properties of massive galaxy environments out to $z = 1.6$ can be directly measured from these integrated profiles. For example, these profiles can be directly compared with estimates of galaxy pair fractions (e.g., Le Fèvre et al. 2000; Patton et al. 2002; Lin et al. 2004; Bell et al. 2006; Kartaltepe et al. 2007; Bluck et al. 2009; Bundy et al. 2009; López-Sanjuan et al. 2012). Recently, Williams et al. (2011) and Newman et al. (2012) found that roughly 20% of all massive galaxies have a luminous companion with a mass ratio of up to 10:1 and within a projected distance of 30 kpc. The same result can be directly extracted from Figure 5 by reading off an average value of 0.2 galaxies within 30 kpc of the primaries.

In addition to quantifying pair fractions in discrete separation values, the derived cumulative profiles describe the enclosed mass in a range of radii, essentially quantifying the average stellar mass content of studied halos. The total number of galaxies within a mass range of 1:10 and within roughly 400 kpc of the primary is on average 2–3 in all redshift bins. This value suggests that massive primary galaxies have typically resided in group halos in the last 9.5 Gyr and it is comparable to the number of luminous satellites in massive groups from other studies (e.g., Tal et al. 2012a; Quilis & Trujillo 2012). Moreover, the total stellar mass in satellites within the halo virial radius can be inferred from the cumulative profiles and it roughly equals the mass of the primary galaxy itself.

3.5. Profile Redshift Evolution

The average radial profiles of the four redshift bins show a remarkable lack of evolution in shape and overall normalization. Within the measurement scatter, the profiles are consistent with one another on nearly all scales from $z = 1.6$ to $z \sim 0$. The lack of evolution in the number density profiles can be naively taken as evidence for a static model of massive halo evolution. According to the stable clustering model (Davis & Peebles 1977), cluster halos decouple from the large-scale cosmological flow shortly after formation. By that point, the halos are virialized and they show no significant evidence for radial infall. As a consequence, any mergers that involve primary galaxies can only be with other galaxies from the same halo.

In order to test the effect of in-halo mergers on the evolution of the radial number density profile we simulated mergers starting with the highest redshift bin ($1.3 < z < 1.6$) and compared the results to the measured profiles at lower redshifts. Mergers were simulated by excluding galaxies from the radial galaxy distributions in the range $10 < r/\mathrm{kpc} < 400$, essentially allowing satellites to merge with the primary from anywhere in the halo. For an estimate of the average merger rate we utilized the results from van Dokkum et al. (2010), who found that massive primary galaxies have roughly doubled in stellar mass since $z = 2$. Assuming that most of the mass growth takes place via minor mergers with mass ratios less than 10:1 (Tal et al. 2012b), the implied merger rate is roughly 0.5 Gyr^{-1}. Figure 6 shows the modeled profiles at the two lowest NMBS redshifts (dashed lines), as well as the observed profiles (solid lines).

It is clear from Figure 6 that in-halo mergers would have a pronounced effect on the evolution of the radial number density profile. If each primary galaxy underwent mergers at

the estimated rate and no new galaxies were added to the halos on similar scales, the observed profile at $1.3 < z < 1.6$ (solid red line) would evolve into the modeled profiles at $0.9 < z < 1.3$ (dashed green line) and at $0.4 < z < 0.9$ (dashed yellow line). Instead, the observed profile at these redshifts (solid green and yellow lines) are consistent with no evolution at all.

Taken at face value, this analysis supports a static model, suggesting that a significant rate of galaxy mergers within the halo is unlikely on time scales of up to roughly 10 Gyr. However, studies of the stellar mass function of massive galaxies show that such galaxies grow significantly in mass over the same redshift range, mainly through mergers (e.g., Dickinson et al. 2003; Bundy et al. 2006; Drory et al. 2005; Pozzetti et al. 2007; Pérez-Gonzalez et al. 2008; Marchesini et al. 2009). It is therefore evident that truly non-evolving models insufficiently recover the observed evolution of massive primary galaxies and their environments.

4. COMPARISON TO A SEMI-ANALYTIC MODEL

4.1. Density Profiles and Mass Growth

In order to study the evolution of massive galaxy groups in the last 9 Gyr we examined numerical predictions using the semi-analytic model of Guo et al. (2011, G11). G11 applied a semi-analytic model to the merger trees of the Millennium Simulation (Springel et al. 2005) and improved the treatment of gas dynamics and tidal disruptions compared to previous studies.

For consistency, we first test whether our cumulative number density matching technique indeed identifies progenitors and descendants in G11. We selected modeled galaxies at $z = 1.63$ using our cumulative number density selection criteria and followed their stellar mass evolution at all simulated time points down to $z = 0$. The median growth factor of massive primary galaxies in G11 is roughly 2.4, consistent with the growth that was measured observationally for similarly massive galaxies by van Dokkum et al. (2010). We also followed the simulated mass evolution of the group dark matter halos and compared it to the average ratio between the halo mass of galaxies selected at $z = 0$ and at $z = 1.63$. We found that both simulated and predicted mass growth factors are within 4% of one another with an average halo growth by a factor of roughly 3.7. In short, by matching massive galaxies by their cumulative number density we were able to correctly trace progenitor and descendant halos.

From the galaxy catalogs of G11 we selected all primary galaxies at redshifts $z = 0.06$, 0.62, 1.17, and 1.63, following the same selection criteria as those used for the observed data. We then collapsed the simulation box along one of the physical dimensions and extracted the projected radial distributions of physically associated galaxies around the selected primaries following the method described in Section 2. This approach allows for a direct comparison with the observational results, as the uncertainties associated with the profile extraction procedure are preserved. The gray profile in Figure 3 represents this measurement in the full redshift range, $0.06 < z < 1.63$. The vertical light-gray region in the figure shows the range of virial radius values of the dark-matter halos in which all selected primaries reside, as determined by G11. Finally, the gray curve in Figure 5 shows the integrated number density profiles over the same redshift range. It is evident from Figure 3 that the average modeled and observed profiles agree well with each other on all but the smallest scales. We note that the innermost observational data point (at $r < 10$ kpc) is likely underestimated since galaxies inside this radius are within the FWHM of the average point spread function at $z > 1$.

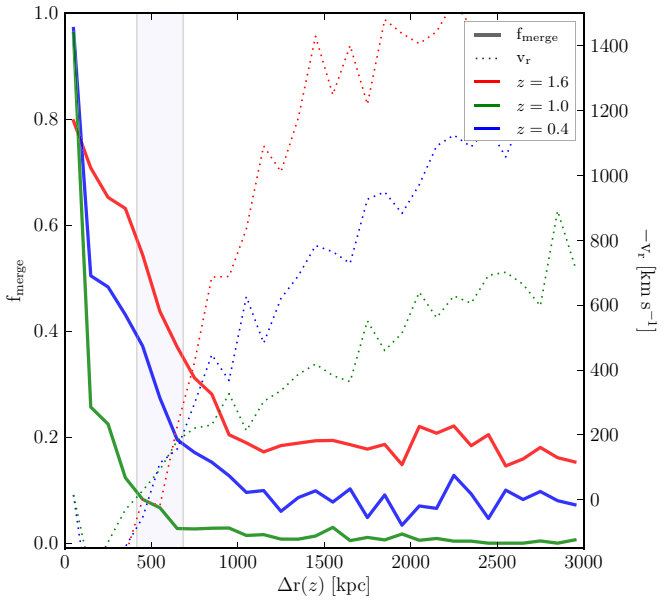

Figure 7. Fate of galaxies around massive primaries in G11. Solid lines represent the fraction of modeled galaxies that merge with their respective primary by $z \sim 0$ as a function of initial separation. Dotted lines show the derived radial component of the velocity vector at the plotted redshift. Three initial redshift measurements, $z = 1.6$, 1.0, and 0.4 are plotted in red, blue, and green, respectively. Galaxies outside of 1000 kpc initially (roughly two virial radii) merge with the primaries at a low rate of less than 20% and move at a high radial velocity. Galaxies inside the halo virial radius merge with the primary at a significantly higher rate with an average infall velocity that is close to zero.

(A color version of this figure is available in the online journal.)

4.2. Fate of Modeled Satellite Galaxies

The good agreement between our result and the theoretical prediction prompted us to further investigate the fate of galaxies around massive primaries by following their merging histories and orbits in the models. To do so, we selected 1000 primary galaxies at $z = 1.63$ from G11 at random, following the selection criteria from Section 2. We then traced the positions of galaxies in 3 Mpc apertures around the primaries that were more massive than one-tenth of the primary mass. We repeated the selection at all output redshifts in the range $0.06 < z < 1.63$ and followed the trajectories of individual galaxies through time. In addition, we determined whether a satellite merges with its primary by $z = 0.06$ using the merger trees of the Millennium Simulation.

The solid lines in Figure 7 show the fraction of satellite galaxies that eventually merge with their primary galaxy as a function of physical separation at $z = 1.6$, 1.0, and 0.4. Galaxies that are found inside the virial radius at any given redshift are significantly more likely to merge with their primary ($f_{merge} > 60\%$ at $z = 1.6$) than galaxies that start off far from the halo ($f_{merge} < 20\%$). However, as is shown in Figure 5, only a small fraction of all galaxies within 3 Mpc are found inside of the group virial radius (~10%). The y-axis on the right-hand side of Figure 7 and the dashed lines show the median radial velocity of satellite galaxies with respect to their primaries, as a function of physical separation. At each redshift we estimated the average streaming velocities by measuring the mean distance between satellites and primaries at two consecutive output

redshifts and dividing the difference between them by the total modeled time span. This measurement gives a rough estimate of the average radial component of the velocity vector in the rest frame of the primary galaxy. Figure 7 shows that galaxies outside of roughly two virial radii fall into the halo with high velocities.

The fate of satellite galaxies in the semi-analytic model of G11 seems to be bimodal. The vast majority of galaxies fall toward the most massive halo galaxy with a high average radial velocity (in agreement with e.g., Tormen 1997; Benson et al. 2005; Khochfar & Burkert 2006; Wetzel 2011) and do not merge with the primary by $z \sim 0$. A small fraction of galaxies have a significantly lower mean radial velocity and they eventually merge with the primary. The probability that a galaxy will merge with its massive primary is inversely proportional to the physical distance between them. At any simulated redshift, most galaxies that are found outside of the halo virial radius will not merge with the primary while a significant fraction of the galaxies found inside of the virial radius will do so by $z \sim 0$.

We note that despite the good agreement between observed and modeled galaxy profiles, the fate of satellite galaxies in numerical simulations should be analyzed with caution. In the context of this study, the disagreement between the evolution of modeled and observed stellar mass functions (e.g., Fontanot 2009; Kajisawa 2009; Cirasuolo 2010; Lu 2012; Mutch 2013) suggests that galaxy merging may be misrepresented in numerical calculations. Therefore, galaxy merging trajectories in observed group halos may be significantly different from modeled ones.

5. SUMMARY AND CONCLUSIONS

The evolution of galaxy properties is determined in large part by the environments in which they reside and the mass density around them. Here we quantified the radial number density profile of galaxies around massive primaries in the redshift range $0.04 < z < 1.6$. We showed that massive galaxies have typically resided in group environments in the past 9.5 Gyr and that they are on average surrounded by 2–3 massive satellite galaxies. We also estimated that the cumulative stellar mass of halo satellites within the virial radius accounts for roughly as much mass as in the massive primary itself, suggesting that the potential for mass growth through in-halo mergers is significant.

Mergers within massive galaxy groups, even at a low rate, are expected to dramatically influence the evolution of observed galaxy distributions in such halos, unless an influx of galaxies continuously repopulates the halo. We compared the number density profiles of massive satellite galaxies in four redshift bins and showed that the profiles are consistent with no evolution out to $z = 1.6$. Although this result may be naively interpreted as evidence for the insignificance of galaxy mergers in group halos, the observed mass growth of massive quiescent galaxies over the same redshift implies that mergers occur at a non-negligible rate. Moreover, results from semi-analytic models suggest that massive primaries continuously merge with satellite galaxies in their halo.

It would also be interesting to compare the observed satellite distributions to predictions from hydrodynamical simulations, such as those of Naab et al. (2007). These models successfully reproduce the build-up of the outer envelopes of massive galaxies through minor mergers (e.g., Naab et al. 2009; Oser et al. 2012; Gabor & Davé 2012; Hilz et al. 2013), and an important question is whether the reservoir of satellite galaxies is also reproduced.

In conclusion, the observed lack of evolution in the number density profiles suggests that there exists a tight balance between mergers and accretion in massive galaxy halos. As satellite galaxies merge with their massive primary, other galaxies get accreted into the halo at a similar rate but on more extreme trajectories. The two competing processes result in a remarkably balanced galaxy distribution out to $r = 3000$ kpc, over the redshift range $0 < z < 1.6$.

This is the first time that an analysis of the evolution of galaxy number density profiles is performed at this redshift and it provides a new observational insight on galaxies in group halos.

We thank Frank van den Bosch, Pascal Oesch and Brad Holden for engaging discussions that contributed to this work.

T.T. is supported by an NSF Astronomy and Astrophysics Postdoctoral Fellowship under award AST-1202667.

We gratefully acknowledge support from the CT Space Grant, NSF grant AST-0807974, and NASA grant NNX11AB08G.

This study makes use of data from the NEWFIRM Medium-Band Survey, a multi-wavelength survey conducted with the NEWFIRM instrument at the KPNO, supported in part by the NSF and NASA.

Funding for the SDSS and SDSS-II has been provided by the Alfred P. Sloan Foundation, the Participating Institutions, the National Science Foundation, the U.S. Department of Energy, the National Aeronautics and Space Administration, the Japanese Monbukagakusho, the Max Planck Society, and the Higher Education Funding Council for England. The SDSS Web site is http://www.sdss.org/.

The SDSS is managed by the Astrophysical Research Consortium for the Participating Institutions. The Participating Institutions are the American Museum of Natural History, Astrophysical Institute Potsdam, University of Basel, University of Cambridge, Case Western Reserve University, University of Chicago, Drexel University, Fermilab, the Institute for Advanced Study, the Japan Participation Group, Johns Hopkins University, the Joint Institute for Nuclear Astrophysics, the Kavli Institute for Particle Astrophysics and Cosmology, the Korean Scientist Group, the Chinese Academy of Sciences (LAMOST), Los Alamos National Laboratory, the Max-Planck-Institute for Astronomy (MPIA), the Max-Planck-Institute for Astrophysics (MPA), New Mexico State University, Ohio State University, University of Pittsburgh, University of Portsmouth, Princeton University, the United States Naval Observatory, and the University of Washington.

REFERENCES

Abazajian, K. N., Adelman-McCarthy, J. K., Agüeros, M. A., et al. 2009, ApJS, 182, 543
Andreon, S., Quintana, H., Tajer, M., Galaz, G., & Surdej, J. 2006, MNRAS, 365, 915
Bell, E. F., Phleps, S., Somerville, R. S., et al. 2006, ApJ, 652, 270
Benson, A. J. 2005, MNRAS, 358, 551
Blanton, M. R., Eisenstein, D., Hogg, D. W., Schlegel, D. J., & Brinkmann, J. 2005, ApJ, 629, 143
Bluck, A. F. L., Conselice, C. J., Bouwens, R. J., et al. 2009, MNRAS, 394, L51
Bolton, A. S., Burles, S., Koopmans, L. V. E., et al. 2008, ApJ, 682, 964
Brammer, G. B., Whitaker, K. E., van Dokkum, P. G., et al. 2009, ApJL, 706, L173
Budzynski, J. M., Koposov, S. E., McCarthy, I. G., McGee, S. L., & Belokurov, V. 2012, MNRAS, 423, 104
Bundy, K., Ellis, R. S., Conselice, C. J., et al. 2006, ApJ, 651, 120
Bundy, K., Fukugita, M., Ellis, R. S., et al. 2009, ApJ, 697, 1369
Cacciato, M., van den Bosch, F. C., More, S., Mo, H., & Yang, X. 2013, MNRAS, 430, 767

Cirasuolo, M., McLure, R. J., Dunlop, J. S., et al. 2010, MNRAS, 401, 1166
Clemens, M. S., Bressan, A., Nikolic, B., et al. 2006, MNRAS, 370, 702
Conroy, C., Gunn, J. E., & White, M. 2009, ApJ, 699, 486
Davis, M., & Peebles, P. J. E. 1977, ApJS, 34, 425
Dickinson, M., Papovich, C., Ferguson, H. C., & Budavári, T. 2003, ApJ, 587, 25
Diener, C., Lilly, S. J., Knobel, C., et al. 2013, ApJ, 765, 109
Dressler, A. 1980, ApJ, 236, 351
Drory, N., Salvato, M., Gabasch, A., et al. 2005, ApJL, 619, L131
Fontanot, F., De Lucia, G., Monaco, P., Somerville, R. S., & Santini, P. 2009, MNRAS, 397, 1776
Gabor, J. M., & Davé, R. 2012, MNRAS, 427, 1816
Gao, L., Loeb, A., Peebles, P. J. E., White, S. D. M., & Jenkins, A. 2004, ApJ, 614, 17
Gavazzi, R., Treu, T., Rhodes, J. D., et al. 2007, ApJ, 667, 176
Guo, Q., Cole, S., Eke, V., Frenk, C., & Helly, J. 2013, arXiv:1301.3134
Guo, Q., White, S., Boylan-Kolchin, M., et al. 2011, MNRAS, 413, 101
Hilz, M., Naab, T., & Ostriker, J. P. 2013, MNRAS, 429, 2924
Hogg, D. W., Blanton, M. R., Brinchmann, J., et al. 2004, ApJL, 601, L29
Holden, B. P., Illingworth, G. D., Franx, M., et al. 2007, ApJ, 670, 190
Jiang, C., Jing, Y., & Li, C. 2012, ApJ, 760, 16
Kajisawa, M., Ichikawa, T., Tanaka, I., et al. 2009, ApJ, 702, 1393
Kartaltepe, J. S., Sanders, D. B., Scoville, N. Z., et al. 2007, ApJS, 172, 320
Kauffmann, G., White, S. D. M., Heckman, T. M., et al. 2004, MNRAS, 353, 713
Khochfar, S., & Burkert, A. 2006, A&A, 445, 403
Knobel, C., Lilly, S. J., Iovino, A., et al. 2012, ApJ, 753, 121
Le Fèvre, O., Abraham, R., Lilly, S. J., et al. 2000, MNRAS, 311, 565
Leja, J., van Dokkum, P., & Franx, M. 2013, ApJ, 766, 33
Lin, L., Koo, D. C., Willmer, C. N. A., et al. 2004, ApJL, 617, L9
López-Sanjuan, C., Le Fèvre, O., Ilbert, O., et al. 2012, A&A, 548, 7
Lu, Y., Mo, H. J., Katz, N., & Weinberg, M. D. 2012, MNRAS, 421, 1779
Madore, B. F., Freedman, W. L., & Bothun, G. D. 2004, ApJ, 607, 810
Mandelbaum, R., Seljak, U., Kauffmann, G., Hirata, C. M., & Brinkmann, J. 2006, MNRAS, 368, 715
Marchesini, D., van Dokkum, P. G., Förster Schreiber, N. M., et al. 2009, ApJ, 701, 1765
Mármol-Queraltó, E., Trujillo, I., Pérez-González, P. G., Varela, J., & Barro, G. 2012, MNRAS, 422, 2187
Mármol-Queraltó, E., Trujillo, I., Villar, V., Barro, G., & Pérez-González, P. G. 2013, MNRAS, 429, 792
Masjedi, M., Hogg, D. W., & Blanton, M. R. 2008, ApJ, 679, 260
Masjedi, M., Hogg, D. W., Cool, R. J., et al. 2006, ApJ, 644, 54
Mutch, S. J., Poole, G. B., & Croton, D. J. 2013, MNRAS, 428, 2001
Muzzin, A., Marchesini, D., van Dokkum, P. G., et al. 2009, ApJ, 701, 1839
Naab, T., Johansson, P. H., & Ostriker, J. P. 2009, ApJL, 699, L178
Naab, T., Johansson, P. H., Ostriker, J. P., & Efstathiou, G. 2007, ApJ, 658, 710
Navarro, J. F., Frenk, C. S., & White, S. D. M. 1997, ApJ, 490, 493
Newman, A. B., Ellis, R. S., Bundy, K., & Treu, T. 2012, ApJ, 746, 162
Nierenberg, A. M., Auger, M. W., Treu, T., et al. 2012, ApJ, 752, 99
Oemler, A. 1974, ApJ, 194, 1
Oser, L., Naab, T., Ostriker, J. P., & Johansson, P. H. 2012, ApJ, 744, 63
Papovich, C., Finkelstein, S. L., Ferguson, H. C., Lotz, J. M., & Giavalisco, M. 2011, MNRAS, 412, 1123
Patel, S. G., Holden, B. P., Kelson, D. D., Illingworth, G. D., & Franx, M. 2009, ApJL, 705, L67
Patel, S. G., Kelson, D. D., Holden, B. P., Franx, M., & Illingworth, G. D. 2011, ApJ, 735, 53
Patel, S. G., van Dokkum, P. G., Franx, M., et al. 2013, ApJ, 766, 15
Patton, D. R., Pritchet, C. J., Carlberg, R. G., et al. 2002, ApJ, 565, 208
Peng, Y.-j., Lilly, S. J., Kova, K., et al. 2010, ApJ, 721, 193
Pérez-González, P. G., Rieke, G. H., Villar, V., et al. 2008, ApJ, 675, 234
Pozzetti, L., Bolzonella, M., Lamareille, F., et al. 2007, A&A, 474, 443
Quadri, R. F., Williams, R. J., Franx, M., & Hildebrandt, H. 2012, ApJ, 744, 88
Quilis, V., & Trujillo, I. 2012, ApJL, 752, L19
Skibba, R. A., & Sheth, R. K. 2009, MNRAS, 392, 1080
Springel, V., White, S. D. M., Jenkins, A., et al. 2005, Natur, 435, 629
Tal, T., Wake, D. A., & van Dokkum, P. G. 2012a, ApJL, 751, L5
Tal, T., Wake, D. A., van Dokkum, P. G., et al. 2012b, ApJ, 746, 138
Thomas, D., Maraston, C., Bender, R., & Mendes de Oliveira, C. 2005, ApJ, 621, 673
Tormen, G. 1997, MNRAS, 290, 411
van den Bosch, F. C., Aquino, D., Yang, X., et al. 2008, MNRAS, 387, 79
van Dokkum, P. G., Labbé, I., Marchesini, D., et al. 2009, PASP, 121, 2
van Dokkum, P. G., Whitaker, K. E., Brammer, G., et al. 2010, ApJ, 709, 1018
Wake, D. A., Sheth, R. K., Nichol, R. C., et al. 2008, MNRAS, 387, 1045
Wake, D. A., Whitaker, K. E., Labbé, I., et al. 2011, ApJ, 728, 46
Wang, W., & White, S. D. M. 2012, MNRAS, 424, 2574
Watson, D. F., Berlind, A. A., McBride, C. K., Hogg, D. W., & Jiang, T. 2012, ApJ, 749, 83
Wetzel, A. R. 2011, MNRAS, 412, 49
Whitaker, K. E., Labbé, I., van Dokkum, P. G., et al. 2011, ApJ, 735, 86
Williams, R. J., Quadri, R. F., & Franx, M. 2011, ApJL, 738, L25
York, D. G., Adelman, J., Anderson, J. E., et al. 2000, AJ, 120, 1579
Zehavi, I., Blanton, M. R., Frieman, J. A., et al. 2002, ApJ, 571, 172
Zehavi, I., Zheng, Z., Weinberg, D. H., et al. 2011, ApJ, 736, 59